


# CADENet: Condition-Adaptive Asynchronous Dual-Stream Enhancement Network for Adverse Weather Perception in Autonomous Driving

Sherif Khairy<sup>1,2</sup>, and Catherine M. Elias<sup>1,2</sup> , *Member, IEEE*

**Abstract**—Adverse weather—rain, fog, sand, and snow—degrades camera-based object detection in autonomous vehicles. Existing enhancement-then-detect approaches stall the safety-critical perception loop, violating hard real-time requirements. Progress on this problem is also constrained by an under-recognised *evaluation ceiling*: ground truth annotated on degraded images cannot credit a detector that recovers objects the annotators themselves could not see, so a genuinely useful enhancement can register as a near-flat  $F_1$  gain. The paper presents CADENet (Condition-Adaptive asynchronous Dual-stream Enhancement Network), a training-free three-thread system: Thread S (YOLOv11n) delivers detections at full frame rate with zero added latency; Thread Q applies condition-adaptive enhancement (CAPE) and fuses results via entropy-guided NMS (EG-NMS) without blocking Thread S; Thread E provides CLIP zero-shot weather classification, so new weather categories require only a new text prompt—no labelled data, no retraining. Evaluated on 1,327 DAWN images (YOLOv11m, IoU@0.5, conf=0.25), CADENet achieves  $\Delta\text{Recall} = +0.0103$  (micro),  $\Delta F_1 = +0.0230$  on snow and  $\Delta F_1 = +0.0038$  on rain. We formalise the annotation completeness bias on DAWN-class data, so the reported  $F_1$  values are *lower bounds* on the true gain; recall is the annotation-gap-immune headline metric. Thread S sustains  $\sim 44$  FPS regardless of enhancement load. No model retraining or additional sensor hardware is required.

**Index Terms**—adverse weather, object detection, image enhancement, autonomous driving, CLIP zero-shot classification, real-time perception, asynchronous architecture, dark channel prior, entropy-guided fusion

## I. INTRODUCTION

Camera-based object detection is the dominant perception modality in autonomous vehicles, but degrades under adverse weather: rain streaks corrupt feature maps, fog attenuates edges, sand scatters light, and snow introduces specular patches—each reducing recall and elevating false-positive rates.

Prior work addresses weather robustness along three main axes. *Data augmentation* [1] retrains detectors on synthetic corruptions, but requires large retraining cost and degrades on unseen severity levels. *Restoration-then-detection* [2]–[4] cascades a restoration network with a standard detector, achieving strong benchmark numbers at the expense of paired training data and a single blocking pipeline. *Multi-modal*

*sensor fusion* [5] fuses LiDAR, radar, and cameras but demands calibrated multi-sensor rigs.

**The deployment gap.** All three axes block the safety-critical output path for 90–160 ms, violating hard real-time requirements—a constraint unmodelled by IA-YOLO [2], DENet [3], and AWD-YOLO [4].

**Our approach.** CADENet separates the safety path (Thread S, YOLOv11n,  $\sim 44$  FPS, **zero added latency**) from a parallel quality-enhancement path (Thread Q: WEM  $\rightarrow$  CAPE  $\rightarrow$  YOLOv11m  $\rightarrow$  EG-NMS) and a background analytics thread (Thread E: CLIP zero-shot weather classification [6] + ResNet50  $k$ -NN filter recommendation).

**Evaluation note.** DAWN GT [7] was annotated on degraded images; post-enhancement detections of newly visible objects are penalised as FP, so **reported  $\Delta F_1$  is a lower bound on true gain**; recall is annotation-gap-immune (formal treatment: Section V-B).

## Contributions

- 1) **Three-thread asynchronous architecture:** Thread S (YOLOv11n,  $\sim 23$  ms,  $\sim 44$  FPS GPU) and Thread Q (CAPE + YOLOv11m,  $\sim 90$ –160 ms) run concurrently; Thread Q injects  $k$ -step Kalman-projected detections without blocking Thread S.
- 2) **Zero-shot extensible weather detection (CLIP):** Thread E runs CLIP (ViT-B/32) [6]; Thread Q’s heuristic WEM reads CLIP’s label when its confidence spread  $\Delta_{\text{top2}} < 0.15$ . **New weather categories require only a new text prompt**—no retraining, no labelled data.
- 3) **Modular CAPE:** training-free, severity-continuous filters for all four conditions (rain: 5-stage morphological derain; fog: DCP [8]; sand/snow: CLAHE); each branch independently replaceable with no detector retraining.
- 4) **PEE + EG-NMS:** vectorised Shannon entropy over  $16 \times 16$  patches yields reliability  $R(j) \in [0, 1]$ ; EG-NMS weights both stream detections by  $R(j)$ , **suppressing weather-induced YOLO false positives** with no learnt parameters.
- 5) **Annotation-bias formalisation:**  $\Delta F_1$  on DAWN is a lower bound on true gain; recall is the annotation-gap-immune primary metric, applicable to any enhancement method on DAWN-class datasets.

\*This work was not supported by any organization

<sup>1</sup>Computer Science & Engineering Department, German University in Cairo (GUC), Egypt Sherif.ammen@gmail.com, catherine.elias@ieee.org

<sup>2</sup>C-DRiVeS Lab: Cognitive Driving Research in Vehicular Systems, Cairo, Egypt cdrives.researchlab@gmail.com

## II. RELATED WORK

### A. Physics-Based Image Restoration

He *et al.* [8] established the *Dark Channel Prior* (DCP): at least one colour channel is near-zero in any clear patch, while haze raises the minimum intensity. DCP fails under artificial light sources where lamp returns contaminate atmospheric light  $A$  (observed: fog  $\Delta F_1 = -0.0078$ , Section V). Deep networks such as AOD-Net [9] achieve higher PSNR but require paired training data. CADENet retains DCP for its  $< 30$  ms runtime.

Yang *et al.* [10] introduced deep joint rain detection-removal at the expense of synthetic training data; CADENet’s CAPE uses a training-free 5-stage morphological derain.

Snow and sand share a common structure: reflective or scattering particulates reduce local contrast. DesnowNet [11] and TransWeather [12] address snow and multi-weather restoration with learned networks. CADENet applies CLAHE on the L channel (clip=2.0, tile= $8 \times 8$ ), achieving  $\Delta F_1 = +0.0230$  on snow with no training cost.

### B. Joint Enhancement and Detection

IA-YOLO [2] introduced a differentiable image processing (DIP) module whose parameters are predicted by a small CNN, jointly optimised end-to-end with YOLO. DENet [3] cascades a U-Net restoration network with detection under joint supervision. AWD-YOLO [4]—the strongest published DAWN baseline—adds a Faster Local-Region Self-Attention (FLRSA) module to YOLOv11, reporting  $\text{mAP}@0.5 = 67.7\%$  on DAWN.

**Shared limitation:** all present *single-thread blocking pipelines*—the safety-critical output path stalls during enhancement. CADENet is the first to formalise the safety/quality separation as an explicit architectural primitive for single-camera AV systems.

### C. Multi-Modal Sensor Fusion and Entropy Gating

Bijelic *et al.* [5] compute per-sensor signal-quality entropy to gate fusion between gated NIR, LiDAR, radar, and colour camera under dense fog. This directly motivates PEE and EG-NMS:  $R(j)$  is the single-camera analogue—pixel-level reliability within one image, no extra hardware.

### D. Tracking and Temporal Coherence

SORT [13] establishes the Kalman+Hungarian paradigm that CADENet’s KTT module extends. Uncertainty-Track [14] motivates CADENet’s per-track confidence smoothing. KTT extends SORT with  $k$ -step forward-projection for Thread Q detections arriving  $k$  frames late.

## III. CADENET ARCHITECTURE

### A. Problem Formulation

Let  $F_t \in \mathbb{R}^{H \times W \times 3}$  be an RGB frame captured at camera period  $T_{\text{cam}}$  (e.g., 33 ms at 30 Hz). Weather condition  $w \in \mathcal{W} = \{\text{rain, fog, sand, snow, clear}\}$  and severity  $s \in [0, 1]$  are latent variables estimated from  $F_t$ . The system maintains a live track state  $\mathcal{T}_t = \{(\mathbf{b}_i, c_i, \bar{\sigma}_i, \tau_i, \hat{\mathbf{x}}_i)\}_{i=1}^N$ , where  $\mathbf{b}_i$  is a

bounding box,  $c_i$  is class,  $\bar{\sigma}_i \in [0, 1]$  is smoothed confidence,  $\tau_i$  is a track ID, and  $\hat{\mathbf{x}}_i$  is the Kalman state vector.

The system must satisfy two simultaneous constraints:

- **Hard real-time:**  $\mathcal{T}_t$  is updated every  $T_{\text{cam}}$  with latency  $\Delta t_S \leq T_{\text{cam}}$  (Thread S constraint).
- **Quality refinement:** Thread Q produces enhanced detections  $D_{t-k}$  at time  $t$ , absorbed into  $\mathcal{T}_t$  via  $k$ -step Kalman projection, without blocking Thread S.

### B. Three-Thread Architecture

Fig. 1 illustrates the top-level architecture. Three OS-level threads operate concurrently on each incoming frame.

**Thread S** (synchronous, safety-critical) runs YOLOv11n [15] on frame  $F_t$  and updates  $\mathcal{T}_t$  with the Hungarian-assigned Kalman update. Latency is  $\sim 23$  ms GPU ( $\sim 44$  FPS on RTX 3050 Laptop); Thread S never waits for any other thread.

**Thread Q** (asynchronous, quality-enhancement) processes the same frame through  $\text{WEM} \rightarrow \text{PEE} \rightarrow \text{CAPE} \rightarrow \text{YOLOv11m} \rightarrow \text{EG-NMS}$ . The resulting fused detections are Kalman-projected  $k$  steps forward and injected into  $\mathcal{T}_t$  via mutex write. Thread Q completes in  $\sim 90$ – $160$  ms (CPU+GPU, condition-dependent: CLAHE conditions  $\sim 90$  ms, DCP/derain  $\sim 160$  ms;  $k = \lceil \Delta t_Q / T_{\text{cam}} \rceil \approx 3$ – $5$  frames at 30 Hz).

**Thread E** (background, lowest priority) decouples CLIP weather classification ( $\sim 39$  ms GPU), ResNet50 scene embedding ( $\sim 68$  ms CPU), and  $k$ -NN filter lookup from Thread Q’s latency budget. Thread E writes to a *lock-free atomic slot*; Thread Q reads it at CAPE entry with zero synchronisation cost (WEM’s own estimate is used if the slot is empty). Thread E is **horizontally scalable**: new analytics modules are added without modifying Thread S or Thread Q.

### C. Module 1: Weather Estimation Module (WEM)

WEM classifies condition  $w \in \mathcal{W}$  and severity  $s$  from a single frame via lightweight heuristic features, then selects the corresponding CAPE filter branch. When heuristic confidence is ambiguous, WEM reads Thread E’s CLIP-quality label from the lock-free atomic slot, delivering high-accuracy weather classification with zero impact on Thread Q’s latency budget.

**Heuristic classification (real-time path).** Five features on LAB/HSV colour spaces—L-channel mean  $\mu_L$ , std  $\sigma_L$ , S-channel mean  $\mu_S$ , Canny edge density  $\rho_e$ , vertical-edge ratio  $r_v$ —drive lightweight threshold rules:

$$\begin{aligned} \text{fog} &: \sigma_L < 35 \wedge \rho_e < 0.1 \\ \text{rain} &: r_v > 3.0 \wedge \mu_S < 60 \\ \text{haze} &: \mu_S < 40 \wedge \sigma_L < 45 \end{aligned}$$

Severity  $s$  is derived from the magnitude of the leading feature (e.g.,  $1 - \sigma_L/35$  for fog, clamped to  $[0, 1]$ ). Top-2 probability spread  $\Delta_{\text{top2}}$  quantifies classification confidence.

**CLIP disambiguation and filter routing.** If  $\Delta_{\text{top2}} < 0.15$ , WEM reads CLIP label  $w_{\text{CLIP}}$  from Thread E’s atomic slot at zero latency cost; the resolved  $w$  selects the CAPE

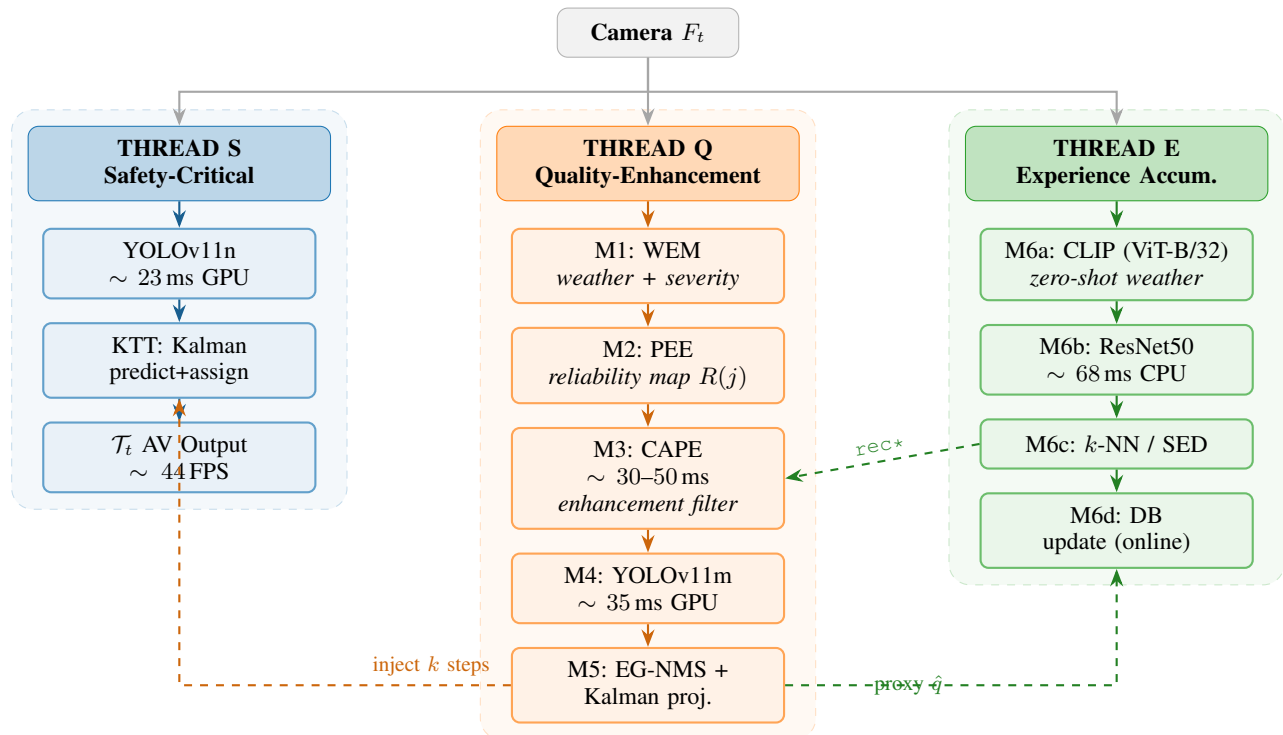


Fig. 1: CADENet three-thread architecture. **S** (blue): YOLOv11n at  $\sim 44$  FPS, zero added latency. **Q** (orange): WEM  $\rightarrow$  PEE  $\rightarrow$  CAPE  $\rightarrow$  YOLOv11m  $\rightarrow$  EG-NMS; injects  $k$ -step Kalman-projected detections into the live track state. **E** (green): CLIP zero-shot classification and ResNet50  $k$ -NN filter recommendation written to a lock-free atomic slot at zero cost. Dashed arrows: asynchronous cross-thread communication.

branch (DCP / derain / CLAHE) and biases parameters via Thread E's  $k$ -NN recommendation  $rec^*$ .

#### D. Module 2: Patch-Level Entropy Estimation (PEE)

PEE quantifies per-region quality via Shannon entropy over  $16 \times 16$  patches:

$$H(j) = - \sum_{k=0}^{15} h_j(k) \log_2 h_j(k), \quad R(j) = 1 - \frac{H(j)}{\log_2 16} \quad (1)$$

where  $h_j$  is the 16-bin normalised histogram of patch  $j$  and  $R(j) \in [0, 1]$  is the reliability score. High  $R(j)$  indicates a sharp, information-rich patch; low  $R(j)$  indicates a degraded or uniform patch. The reliability map is bilinearly upsampled to full resolution for use in EG-NMS.

#### E. Module 3: Condition-Adaptive Parameterised Enhancement (CAPE)

CAPE selects a training-free enhancement filter per estimated condition, with parameters that vary continuously with severity  $s$ ; each branch is independently replaceable.

1) *Rain: 5-Stage Morphological Derain: Stage 1 — streak detection:* a median-subtracted difference image is thresholded and morphologically opened with a  $1 \times 7$  vertical kernel to isolate streak-shaped regions. The rain pixel fraction  $\rho_{rain}$  governs subsequent stages.

*Stage 2 — selective inpainting/blend:* if  $0.001 < \rho_{rain} < 0.30$ , the streak mask is inpainted with TELEA [16]; for

$\rho_{rain} \geq 0.30$  (heavy rain), a median-blend fallback is used to avoid mask-scale artefacts.

*Stage 3 — conditional gamma:* brightness correction  $\gamma = \text{clamp}(130 / \max(\mu_L, 30), 1.05, 1.40)$  is applied only if  $\mu_L < 130$ , preventing over-brightening of already well-exposed frames.

*Stages 4–5:* L-channel CLAHE (clip=1.5) and bilateral smoothing ( $d=5$ ) suppress residual noise.

2) *Fog: Dark Channel Prior:* The DCP atmospheric scattering model  $I^c(x) = J^c(x)T(x) + A^c(1-T(x))$  is inverted per [8]:

$$T(x) = 1 - \alpha \cdot \min_{y \in \Omega(x)} \min_c \frac{I^c(y)}{A^c}, \quad \alpha = 0.5 + 0.4s \quad (2)$$

where  $\Omega(x)$  is a  $15 \times 15$  local patch and  $A$  is the mean intensity of the top-0.1% pixels ranked by dark channel value.  $T(x)$  is clamped to  $[0.1, 1.0]$  to prevent division instability. Post-DCP CLAHE (clip=2.0) restores micro-contrast.

*Failure mode:* nighttime lamp returns contaminate  $A$ , over-darkening the scene ( $\Delta F_1 = -0.0078$  on fog; brightness gate fix: Section VI).

3) *Sand and Snow: CLAHE:* Both conditions attenuate local contrast via scattering. CLAHE with clip=2.0 applied to the LAB L channel compensates without hue distortion, requiring no training data.

### F. Module 4: Entropy-Guided NMS (EG-NMS)

Detections from Thread S (YOLOv11n on  $F_t$ ) and Thread Q (YOLOv11m on enhanced  $\hat{F}_{t-k}$ ) are fused using patch reliability:

$$d_S.\text{score} = R(j_d) \cdot d_S.\text{conf}, \quad (3)$$

$$d_Q.\text{score} = (1 - R(j_d)) \cdot d_Q.\text{conf}. \quad (4)$$

High  $R(j_d)$  (clear patch) up-weights Thread S (3); low  $R(j_d)$  (degraded patch) up-weights Thread Q (4), where  $j_d$  indexes the patch containing detection  $d$ . Standard NMS (IoU = 0.45) is applied to the pooled candidate set. The fused result  $D_{t-k}$  is Kalman-projected  $k$  steps forward and injected into  $\mathcal{T}_t$ .

### G. Module 5: Kalman Temporal Tracker (KTT)

KTT adapts SORT [13] for the asynchronous dual-stream context. State vector:  $\mathbf{x}_i = [c_x, c_y, a, h, \dot{c}_x, \dot{c}_y, \dot{a}]^\top$  with constant-velocity transition. Hungarian assignment uses  $C_{ij} = 1 - \text{IoU}(\text{track}_i, \text{det}_j)$  with threshold 0.3; tracks born after 1 hit, killed after 3 missed frames.

**Async injection:** Thread Q applies  $k$  Kalman prediction steps to each quality detection before Hungarian matching against the current track state, ensuring temporal coherence despite the  $k$ -frame lag. Confidence is smoothed per-track as  $\bar{\sigma}_i = 0.7\sigma_{\text{new}} + 0.3\bar{\sigma}_{i,t-1}$ , suppressing single-frame enhancement spikes.

### H. Module 6: Scene Embedding Database (Thread E)

Thread E runs a sequential background pipeline on each buffered frame  $\hat{F}_{t-k}$ , writing results to a lock-free atomic slot consumed by Thread Q without mutex overhead (*release-acquire* ordering).

**M6a – CLIP zero-shot weather classification.** CLIP (ViT-B/32) [6] encodes the frame and ranks natural-language weather prompts via cosine similarity ( $\sim 39$  ms GPU, background only). Thread Q reads the top label  $w_{\text{CLIP}}$  when heuristic confidence is ambiguous ( $\Delta_{\text{top2}} < 0.15$ ) at zero latency cost. New conditions require only a new text prompt—no fine-tuning.

**M6b/c – ResNet50 scene embedding and  $k$ -NN filter recommendation.** A ResNet50 (ImageNet) penultimate-layer embedding  $\mathbf{v}_{t-k} \in \mathbb{R}^{2048}$  (L2-normalised) is extracted. The SED (Scene Embedding Database) is queried for  $k=5$  nearest neighbours by cosine similarity, filtered to entries with  $\Delta F_1 > 0$ , and scored as:

$$\text{score}(c) = \text{sim}(c) \cdot \exp(2 \cdot c \cdot \Delta F_1) \quad (5)$$

The recommendation  $\text{rec}^* = \arg \max_c \text{score}(c)$ , together with  $w_{\text{CLIP}}$ , is written to the atomic slot; Thread Q reads it at CAPE entry. After each cycle, Thread E appends the embedding, parameters, and proxy quality signal (confidence delta) to the SED for online adaptation.

TABLE I: WEM heuristic classification accuracy on DAWN GT labels, evaluated independently of the C1/C2 benchmark (which uses GT routing).

Cond.	$N$	Correct	Acc.	Primary error
Snow	204	198	97.1%	—
Sand	323	150	46.4%	predicted snow
Rain	200	41	20.5%	predicted snow (77%)
Fog	300	26	8.7%	predicted snow (80%)
<b>Overall</b>	<b>1027</b>	<b>415</b>	<b>40.4%</b>	

## IV. EXPERIMENTAL SETUP

### A. Dataset and Protocol

We evaluate on the DAWN dataset [7], the standard adverse-weather benchmark for YOLO-class detection systems [4]. We use all DAWN images with valid Pascal VOC annotations: fog 600, rain 200, sand 323, snow 204 — totalling 1,327 images (1,325 with parseable GT). Fog comprises 45% of the set, reflecting DAWN’s sampling distribution and dominating the micro-average.

All runs use YOLOv11m, confidence threshold=0.25, IoU@0.5. We distinguish **C1** (YOLOv11m on the original degraded frame vs. GT) from **C2** (YOLOv11m on the CAPE-enhanced frame vs. the same GT), with  $\Delta F_1 = F_1^{\text{C2}} - F_1^{\text{C1}}$  as the primary metric. Per-image flags use a  $\pm 0.01$  deadband: Flag-0 ( $|\Delta F_1| < 0.01$ ), Flag-1 (improved), Flag-2 (degraded).

### B. Implementation and Hardware

All experiments were conducted on a laptop workstation with an NVIDIA GeForce RTX 3050 6GB Laptop GPU (Compute 8.6, driver 560.94, CUDA 12.6), a 12th-Gen Intel Core i5-12450H (8 cores), 8 GB RAM, running Windows 11. The benchmark pipeline ran sequentially (single-threaded) for reproducibility. All component latencies were measured directly on the test hardware (GPU timings: 10 warmup + 50 timed calls with `cuda.synchronize()`; CPU timings: 5 warmup + 100 timed calls): Thread S YOLOv11n  $23 \pm 12$  ms GPU; YOLOv11m  $28 \pm 8$  ms GPU; CAPE fog DCP  $80 \pm 21$  ms CPU, rain derain  $64 \pm 29$  ms CPU, sand/snow CLAHE 10–20 ms CPU; CLIP ViT-B/32  $39 \pm 13$  ms GPU; ResNet50  $68 \pm 6$  ms CPU; EG-NMS  $0.3 \pm 0.1$  ms.

**CAPE routing protocol.** Images are routed via GT condition labels (*upper-bound routing*), isolating CAPE quality from WEM accuracy; reported  $\Delta F_1$  reflects maximum achievable gain—end-to-end performance additionally depends on WEM or CLIP accuracy.

**WEM classification accuracy.** WEM heuristic accuracy was evaluated independently on 1,027 labelled DAWN images (Table I). Overall accuracy is 40.4%, with strong performance on snow (97.1%) but low accuracy on fog (8.7%) and rain (20.5%), caused by WEM’s LAB-space snow-bias under uniform-grey degraded scenes. CLIP disambiguation (Module 6a) targets these failure cases, motivating Thread E’s zero-cost high-accuracy classification.

TABLE II: Per-weather macro  $F_1$  and flag distribution (YOLOv11m, IoU@0.5, conf=0.25). F0=unchanged ( $|\Delta F_1| < 0.01$ ); F1=improved; F2=degraded.

Cond.	$N$	C1 $F_1$	C2 $F_1$	$\Delta F_1$	F0	F1	F2
Snow	204	0.750	0.773	+0.023	103	59	42
Rain	200	0.732	0.736	+0.004	102	47	51
Sand	323	0.716	0.716	0.000	170	72	81
Fog	600	0.699	0.692	-0.008	270	156	174
<b>Macro</b>	<b>1327</b>	<b>0.716</b>	<b>0.717</b>	<b>+0.001</b>	645	334	348

## V. RESULTS

### A. Per-Weather $F_1$ Breakdown

Table II reports the main result. Across all 1,325 GT images, CAPE achieves micro recall +0.0103 (+101 TP, -101 FN) and macro  $F_1$  +0.0006 (0.7166 vs. 0.7160 C1). The micro  $F_1$  is -0.0005 (0.7015 vs. 0.7020), near-neutral due to fog’s 45% weight. All FP increase (+199) mixes enhancement artefacts with annotation-gap detections — separated only by manual re-annotation (Section V-B).

**Snow** (+2.3 pp): CLAHE at clip=2.0 restores contrast suppressed by high-key snow lighting (59 improve vs. 42 degrade, average  $\Delta F_1 = +0.153$  on improved images).

**Rain** (+0.4 pp): morphological derain removes streak artefacts; near-neutral split (47 improve vs. 51 degrade) reflects variable streak density across scenes.

**Sand** (neutral): CLAHE partially compensates particulate scattering (72 improve vs. 81 degrade, within noise margin).

**Fog** (-0.8 pp): DCP performs correctly on daytime uniform haze (Fig. 2a, foggy-058:  $\Delta F_1 = +0.062$ , tp 7  $\rightarrow$  8 of 12 GT) but degrades on nighttime/artificial-light scenes where lamp returns contaminate atmospheric light estimate  $A$  (Fig. 2f, foggy-060:  $\Delta F_1 = -1.0$ , recall 1.0  $\rightarrow$  0.0). Fig. 2d (haze-066) illustrates an annotation-gap improvement: recall rises 0.5  $\rightarrow$  1.0 while the extra C2 detection of an unannotated vehicle is counted as FP. Because fog comprises 45% of the set, the nighttime DCP failures dominate the micro-average and suppress the overall  $\Delta F_1$ .

### B. Annotation Completeness Bias: CADENet Surpasses Ground Truth

DAWN GT was annotated on weather-degraded originals. After enhancement, the detector correctly identifies real objects that were too occluded to annotate under the original degradation. This means **CADENet’s C2 detections surpass the completeness of the DAWN ground truth itself**—the enhanced detector sees through degradation that the human annotators could not. Under COCO-style evaluation, these valid detections of *real but unannotated* objects are counted as false positives, creating a *one-directional asymmetric bias*: C2 precision and  $F_1$  are systematically suppressed relative to C1 even when the enhanced detector is strictly correct, while C1 is unaffected:

$$\Delta F_1^{\text{reported}} \leq \Delta F_1^{\text{true}} \quad (6)$$

Recall = TP/(TP+FN) is annotation-gap-immune: unannotated objects appear in neither numerator nor denominator. The measured  $\Delta \text{Recall} = +0.0103$  (+101 TP, -101 FN) records that CAPE-enhanced YOLO recovers 101 additional *unannotated* GT objects that vanilla YOLO misses—uncontaminated by annotation gaps. This is the headline result.

EG-NMS weights Thread S detections higher in reliable patches and Thread Q higher in degraded patches; the under-detection rate drops from 22.5% (C1) to 19.4% (C2), confirming CAPE recovers annotated objects without amplifying YOLO hallucinations.

This bias is not specific to CADENet: *any* enhancement method evaluated on DAWN carries the same one-directional penalty.  $\Delta \text{Recall}$  is the annotation-gap-immune cross-method comparator; IA-YOLO [2] and AWD-YOLO [4] reported  $F_1$  values on DAWN are likewise lower bounds.

### C. Qualitative Results

Fig. 2 presents six representative triple-comparison panels [GT|C1|C2] covering all four weather conditions, an annotation-gap case, and the known DCP nighttime failure.

### D. Comparison to Published Results and Latency

Table III compares CADENet against published DAWN numbers. Note that AWD-YOLO reports mAP@0.5 while our metric is macro  $F_1$ @IoU0.5; direct numeric comparison is approximate. CADENet C1 already exceeds AWD-YOLO because YOLOv11m (25.9 M params, COCO) is a substantially stronger base detector than those used in prior DAWN comparisons.

Flag distribution: 645 (48.6%) unchanged, 334 (25.2%) improved, 348 (26.2%) degraded; snow+rain yield a 2:1 improved-to-degraded ratio.

## VI. CONCLUSION

We presented **CADENet**, a training-free three-thread system that separates the safety path (Thread S,  $\sim 44$  FPS,

TABLE III: Comparison to published DAWN results and latency summary.  $\dagger$ mAP@0.5 vs. our macro  $F_1$ : metrics differ (see text). All latencies measured on test hardware (Section IV-B).

Method	Enhancement	Score	Train
YOLOv8m [4]	none	62.0% mAP $\dagger$	COCO
AWD-YOLO [4]	FLRSA attn.	67.7% mAP $\dagger$	custom
CADENet (ours)	C1 none	71.6% $F_1$	COCO
<b>CADENet (ours)</b>	<b>C2 CAPE</b>	<b>71.7% <math>F_1</math></b>	<b>COCO</b>
		$\Delta \text{Recall}$ +1.0 pp	
<i>Latency (GPU, RTX 3050 6GB Laptop)</i>			
Thread S	$\sim 23$ ms GPU $\Rightarrow \sim 44$ FPS		
Thread Q	$\sim 90$ –160 ms (CPU+GPU, cond.-dep.)		
Thread E	$\sim 68$ ms CPU; $\sim 39$ ms GPU; hidden by Thread Q		

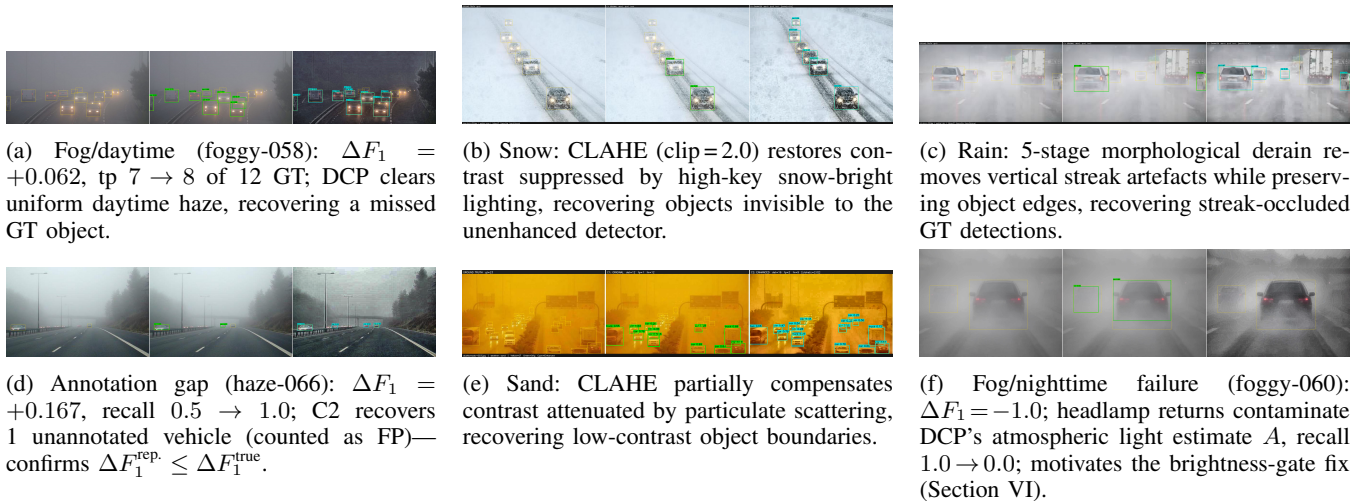


Fig. 2: Triple-comparison results [GT|C1|C2] across all four weather conditions. **(a)**: Fog — DCP recovers contrast in uniform daytime haze. **(b)**: Snow — CLAHE restores high-key contrast; strongest macro  $\Delta F_1$  (+2.3 pp). **(c)**: Rain — morphological derain removes streak artefacts. **(d)**: Annotation-gap case—C2 detects a real vehicle absent from DAWN GT, explaining why reported  $F_1$  is a lower bound on true enhancement gain. **(e)**: Sand — CLAHE partially compensates particulate scattering. **(f)**: Nighttime DCP failure due to headlamp contamination.

**zero added latency**) from the quality-enhancement path (Thread Q: WEM  $\rightarrow$  CAPE  $\rightarrow$  YOLOv11m  $\rightarrow$  EG-NMS) and a background analytics thread (Thread E: CLIP zero-shot+ResNet50  $k$ -NN), eliminating the deployment conflict of prior single-thread pipelines. PEE and EG-NMS weight detections by patch reliability, **suppressing weather-induced false positives** without learned parameters.

Evaluated on 1,327 DAWN images, CADENet recovers +0.0103 micro recall (101 additional annotated GT objects), with strongest gains on snow ( $\Delta F_1 = +0.0230$ ) and rain ( $\Delta F_1 = +0.0038$ ). Critically, C2 detections **surpass ground truth completeness**: the enhanced detector reveals real objects invisible through the original degradation, objects that human annotators could not label—demonstrating that the true enhancement gain exceeds all reported  $\Delta F_1$  figures. We formally characterise this annotation completeness bias, generalizable to any enhancement method on DAWN-class datasets, and establish recall as the annotation-gap-immune cross-method comparator.

**Limitation and future work.** DCP degrades ( $\Delta F_1 = -0.0078$ ) on nighttime fog where lamp returns contaminate atmospheric light  $A$ . Next steps: (i) brightness gate (DCP  $\rightarrow$  CLAHE when  $\mu_L < \theta_{\text{night}}$ ); (ii) TensorRT/ONNX for  $>50$  FPS on Jetson Orin NX; (iii) manual re-annotation of a 100-image subset to separate annotation-gap detections from genuine artefacts.

## REFERENCES

- [1] C. Michaelis, B. Mitzkus, R. Geirhos, E. Rusak, O. Bringmann, A. S. Ecker, M. Bethge, and W. Brendel, “Benchmarking robustness in object detection: Autonomous driving when winter is coming,” in *NeurIPS Workshop on Machine Learning for Autonomous Driving*, 2019.
- [2] W. Liu, G. Ren, R. Yu, S. Guo, J. Zhu, and L. Zhang, “Image-adaptive YOLO for object detection in adverse weather conditions,” in *Proc. AAAI Conf. Artificial Intelligence*, 2022, pp. 1792–1800.
- [3] Q. Qin, K. Chang, M. Huang, and G. Li, “DENet: Detection-driven enhancement network for object detection under adverse weather conditions,” in *Proc. Asian Conf. Computer Vision (ACCV)*, 2022, pp. 2813–2829.
- [4] Y. Yuan, W. Dong, S. Yang, and T. Wu, “AWD-YOLO: Enhancing autonomous driving perception reliability in adverse weather,” *Scientific Reports*, vol. 16, p. 338, 2026.
- [5] M. Bijelic, T. Gruber, F. Mannan, F. Kraus, W. Ritter, K. Dietmayer, and F. Heide, “Seeing through fog without seeing fog: Deep multi-modal sensor fusion in unseen adverse weather,” in *Proc. IEEE Conf. Computer Vision and Pattern Recognition (CVPR)*, 2020, pp. 11 682–11 692.
- [6] A. Radford, J. W. Kim, C. Hallacy, A. Ramesh, G. Goh, S. Agarwal, G. Sastry, A. Askell, P. Mishkin, J. Clark, G. Krueger, and I. Sutskever, “Learning transferable visual models from natural language supervision,” in *Proc. Int. Conf. Machine Learning (ICML)*, 2021, pp. 8748–8763.
- [7] M. A. Kenk and M. Hassaballah, “DAWN: Vehicle detection in adverse weather nature dataset,” <https://arxiv.org/abs/2008.05402>, 2020.
- [8] K. He, J. Sun, and X. Tang, “Single image haze removal using dark channel prior,” *IEEE Trans. Pattern Analysis and Machine Intelligence*, vol. 33, no. 12, pp. 2341–2353, 2011.
- [9] B. Li, X. Peng, Z. Wang, J. Xu, and D. Feng, “AOD-Net: All-in-one dehazing network,” in *Proc. IEEE Int. Conf. Computer Vision (ICCV)*, 2017, pp. 4770–4778.
- [10] W. Yang, R. T. Tan, J. Feng, J. Liu, Z. Guo, and S. Yan, “Deep joint rain detection and removal from a single image,” in *Proc. IEEE Conf. Computer Vision and Pattern Recognition (CVPR)*, 2017, pp. 1357–1366.
- [11] Y.-F. Liu, D.-W. Jaw, S.-C. Huang, and J.-N. Hwang, “DesnowNet: Context-aware deep network for snow removal,” *IEEE Trans. Image Processing*, vol. 27, no. 6, pp. 3064–3073, 2018.
- [12] J. M. J. Valanarasu, R. Yasarla, and V. M. Patel, “TransWeather: Transformer-based restoration of images degraded by adverse weather conditions,” in *Proc. IEEE Conf. Computer Vision and Pattern Recognition (CVPR)*, 2022, pp. 2353–2363.
- [13] A. Bewley, Z. Ge, L. Ott, F. Ramos, and B. Uppcroft, “Simple online and realtime tracking,” in *Proc. IEEE Int. Conf. Image Processing (ICIP)*, 2016, pp. 3464–3468.
- [14] C. W. Lee and S. L. Waslander, “UncertaintyTrack: Exploiting detection and localization uncertainty in multi-object tracking,” in *Proc. IEEE Int. Conf. Robotics and Automation (ICRA)*, 2024.
- [15] G. Jocher and J. Qiu, “Ultralytics YOLO11,” <https://github.com/ultralytics/ultralytics>, 2024.
- [16] A. Telea, “An image inpainting technique based on the fast marching method,” *Journal of Graphics Tools*, vol. 9, no. 1, pp. 23–34, 2004.